

Supporting Information

Tailoring 6FDA-based click cross-linked membranes: modular synthesis and tunable gas separation

Jieun Park,[†] Chang Oh Lee,[†] Ki Jung Kim, Won Seok Chi,^{*} and Hyungwoo Kim^{*}

School of Polymer Science and Engineering, Chonnam National University, 77 Yongbong-ro, Buk-gu, Gwangju 61186, Korea

[†]These authors contributed equally to this work

^{*}Corresponding author e-mails: wschi@jnu.ac.kr (W.S.C.), kimhw@jnu.ac.kr (H.K.)

Contents

General Experimental	S1
Instrumentation.....	S1
Synthetic Procedures and Sample Preparation	S4
Literature Survey.....	S6
NMR Spectra.....	S7
FTIR Spectra.....	S9
Supplementary Photographs.....	S9
Tensile Stress–Strain Curves.....	S10
SEM Images.....	S10
Contact Angle Measurement.....	S11
Plasticization Behavior	S11
Estimation of Fractional Free Volume.....	S12
Gas Permeation Measurement.....	S12
Gas Permeation Properties: Permeability and Selectivity	S15
Gas Permeation Properties: Diffusivity and Diffusivity-Selectivity	S15
Gas Permeation Properties: Solubility and Solubility-Selectivity	S16
References.....	S16

General Experimental

All reactions were performed in flame-dried glassware under a positive pressure of nitrogen unless otherwise noted. Air- and moisture-sensitive liquids were transferred by syringe or stainless steel cannula. H₂, N₂, CH₄, and CO₂ gas cylinders in UHP grade (>99.999%) were purchased from Daesung Synthetic Co., LTD. 6FDA-DAM:DABA (3:2) (6FDD) (M_w = 210 kDa, PDI = 2.50) was purchased from Akron Polymer Systems and used as received.

Instrumentation

Proton nuclear magnetic resonance (¹H NMR) spectra were recorded on a Bruker Ascend 400 MHz spectrometer at 25 °C and processed using MestReNova software. Proton chemical shift are expressed in part per million (ppm, δ scale) and are referenced to

tetramethylsilane ((CH₃)₄Si 0.00 ppm) or to residual protium in the solvent (CDCl₃, δ 7.26 ppm). Data are represented as follows: chemical shift, multiplicity (s = singlet, d = doublet, t = triplet, q = quartet, m = multiplet and/or multiple resonances, br = broad peak), coupling constant in Hertz (Hz), and integration. Carbon nuclear magnetic resonance (¹³C NMR) were recorded using Bruker 400 MHz NMR spectrometer at 25 °C. Carbon chemical shifts are expressed in parts per million (ppm, δ scale) and are referenced to the carbon resonances of the NMR solvent (DMSO-*d*₆, δ 39.53 ppm).

Uniaxial tensile tests were performed using a universal testing machine (UTM) (MCT-2150, A&D, Japan) with a 500-N load cell at 25 °C in air. Tensile samples for the mechanical testing were glued between two slide glass with a superglue for the measurement. Samples for the mechanical testing were prepared to have a size of (width × length × thickness) 5 mm × 10 mm × 0.07 mm for tensile testing. The samples were elongated at a rate of 10 mm min⁻¹ until broken. Then, stress-strain curves were recorded. Young's modulus was obtained from the initial slope of the stress-strain curve in the strain range of 0–10%.

Morphology was observed using a Carl Zeiss SUPRA 55VP scanning electron microscope (SEM) at an accelerating voltage of 2 kV. Before the measurement, the sample was dried in vacuum and coated with a thin platinum layer.

Density of films was determined at 25 °C using an electronic balance (Sartorius, Cubis® II Analytical) which was equipped with a density determination kit (Sartorius, YDK03).

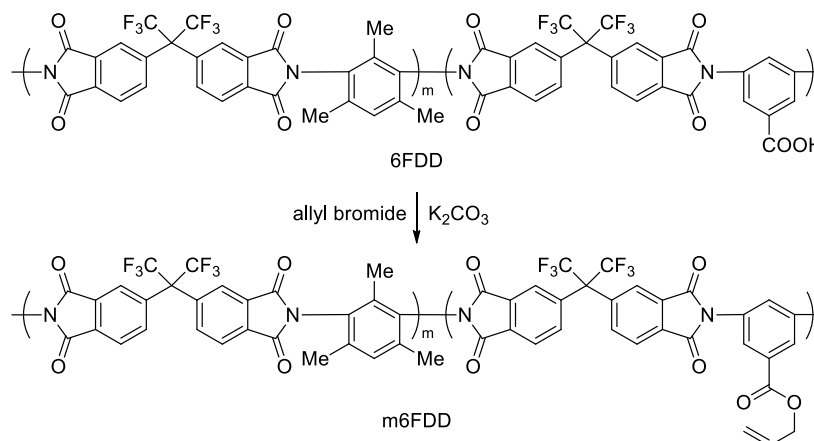
Fourier-transform infrared spectroscopy (FTIR) were performed using an attenuated total reflectance Fourier-transform infrared spectroscopy (ATR-FTIR, IFS66/S, Bruker, USA).

Water Contact angle measurements were conducted using a SurfaceTech GSA-X goniometer at 25 °C in air. The contact angle measurement was performed on a flat surface. The angles were measured immediately after dripping a water droplet on the surface of sample.

X-ray diffraction (XRD) analysis was performed using a PANalytical X'Pert PRO MPD with Cu K α radiation (λ , 1.5406 Å) to determine the crystallinity of materials. The d-spacing values (d) were estimated following the Bragg's law (i.e., $d = \lambda/2 \sin \theta$). All experiments were performed at room temperature.

Synthetic Procedures and Sample Preparation

Synthesis of the modified 6FDD (m6FDD):



Scheme S1. Schematic description of m6FDD.

To a solution of 6FDD (500 mg, 0.18 mmol, 1.0 equiv) in dried *N,N*-dimethylformamide (DMF) (8.68 mL) were added potassium carbonate (49.43 mg, 0.36 mmol, 1.7 equiv) and allyl bromide (36.78 mg, 0.03 mL, 0.30 mmol, 1.7 equiv) in sequence. After stirring at 25 °C for 24 h, the resulting mixture was poured in cold methanol (MeOH) and the precipitate was isolated by filtration. The obtained product was further purified three times by re-precipitation in MeOH after re-dissolving in small amounts of DMF to afford the desired m6FDD as a light pink solid (90 %). 1H NMR (DMSO- d_6 , 400 MHz): δ 8.20–8.17 (m, 15.8 H), 7.95–7.76 (m, overlap, 22.2 H), 7.32 (s, 3.1 H), 6.03 (m, 1.7 H), 5.42 (d, 1.7 H, $J = 16.47$ Hz), 5.28 (d, 1.7 H, $J = 10.32$ Hz), 4.85 (s, 3.5 H), 2.14 (s, 18 H), 1.92 (s, 9 H) (spectrum, Figure S1). ^{13}C NMR (DMSO- d_6 , 100 MHz): δ 166.3, 164.5, 138.8, 138.2, 137.9, 136.9, 133.5, 133.2, 132.8, 131.4, 128.7, 125.2, 124.5, 118.6, 66.1, 65.1, 64.9, 18.1, 14.0 (spectrum Figure S2). The degree of substitution was calculated by 1H NMR spectrum.

Preparation of cross-linked membranes:

The modified polymer m6FDD (150 mg) was dissolved in DMF (1 mL). To this solution were added specific amounts of various thiol cross-linkers and 2-hydroxy-4'-(2-hydroxyethoxy)-2-methylpropiophenone (Irgacure 2959; 3 wt%) as a photoinitiator. The resulting mixtures were dripped on a glass petri dish, irradiated by a UV light (<365 nm) for 5 min, and then covered with aluminum foil with a few holes to achieve slow evaporation. After storing in an oven at 50 °C overnight, the resultant polymer films were formed and recovered from the dish. The free-standing films were further dried overnight under vacuum at 60 °C. After solvent exchange with MeOH for 4 h at rt and following vacuum-drying at 35 °C overnight, flexible and transparent membranes were obtained having a thickness around 70 μm.

Control m6FDD membrane: This un-cross-linked membrane was fabricated following a similar method mentioned above except for using a cross-linker, initiator, and UV irradiation.

Literature Survey

Table S1. A summary of gas separation membranes cross-linked by diverse reaction mechanisms.

Mother polymer	Cross-linking mechanism	Method	ref	
6FDA-based	vinyl polymerization	photo	S1	
	radical generation (decarboxylation)	thermal	S2, S3	
	radical generation (benzophenone)	photo	S4	
	metal coordination	thermal	S5, S6	
	acetalization	thermal	S7	
	condensation	thermal	S6–S8	
	urethane formation	thermal	S9	
	thiol-ene reaction	photo	this work	
Matrimid®-based	metathesis polymerization (diphenylacetylene)	thermal	S10	
	[2+2] cyclization	thermal	S11	
others	polyacrylate-based	vinyl polymerization	photo or thermal	S12, S13
		epoxy-amine reaction	thermal	S14
	polyamide-based	condensation	thermal	S15
	poly(ethylene glycol)-based	urethane formation	thermal	S16

NMR Spectra

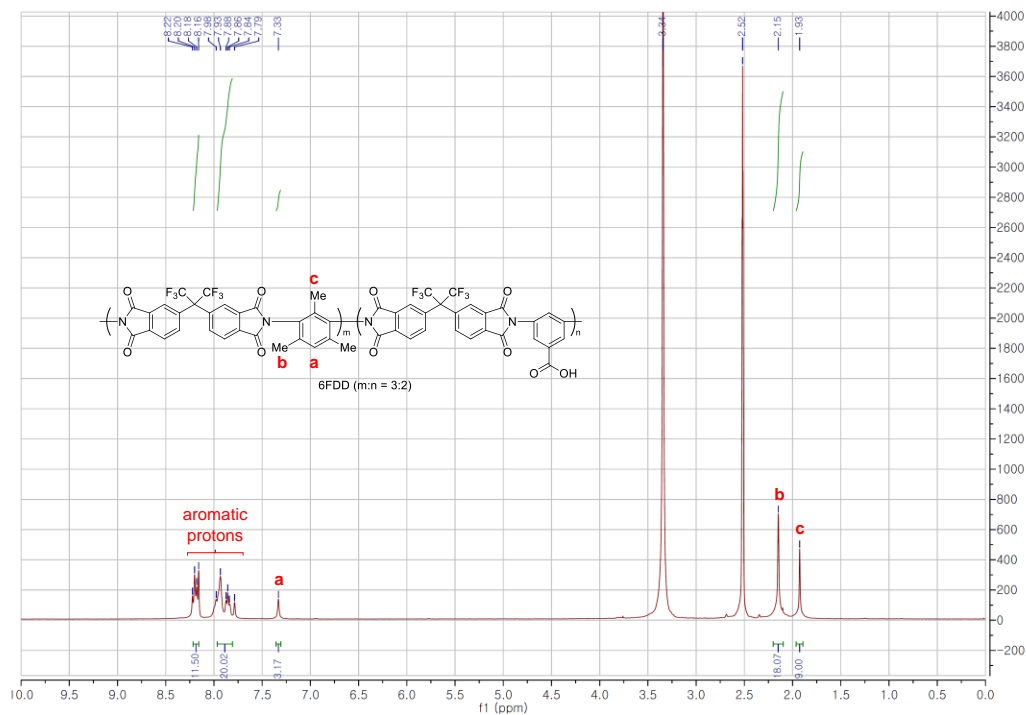


Figure S1. ¹H NMR spectrum of 6FDD

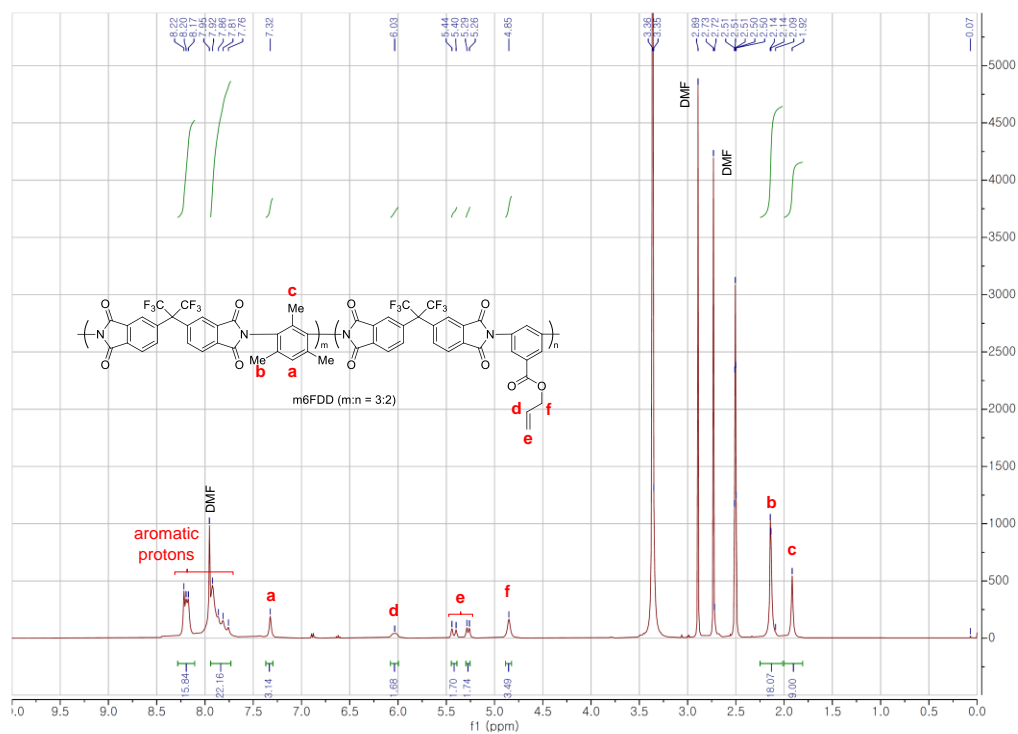


Figure S2. ¹H NMR spectrum of m6FDD.

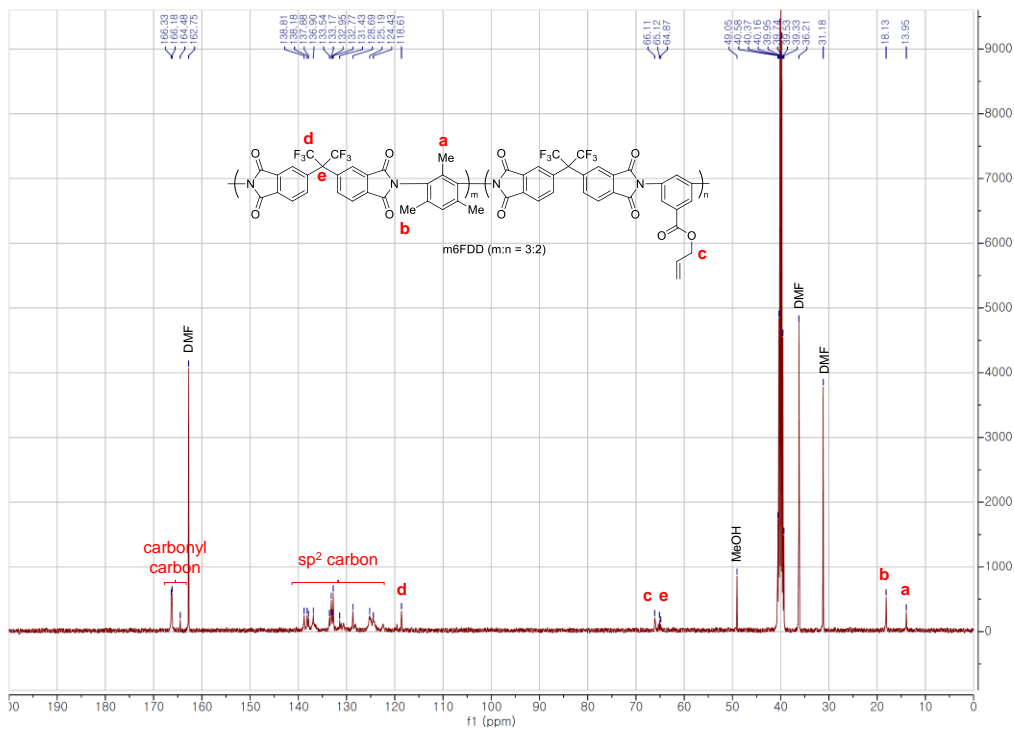


Figure S3. ^{13}C NMR spectrum of m6FDD.

FTIR Spectra

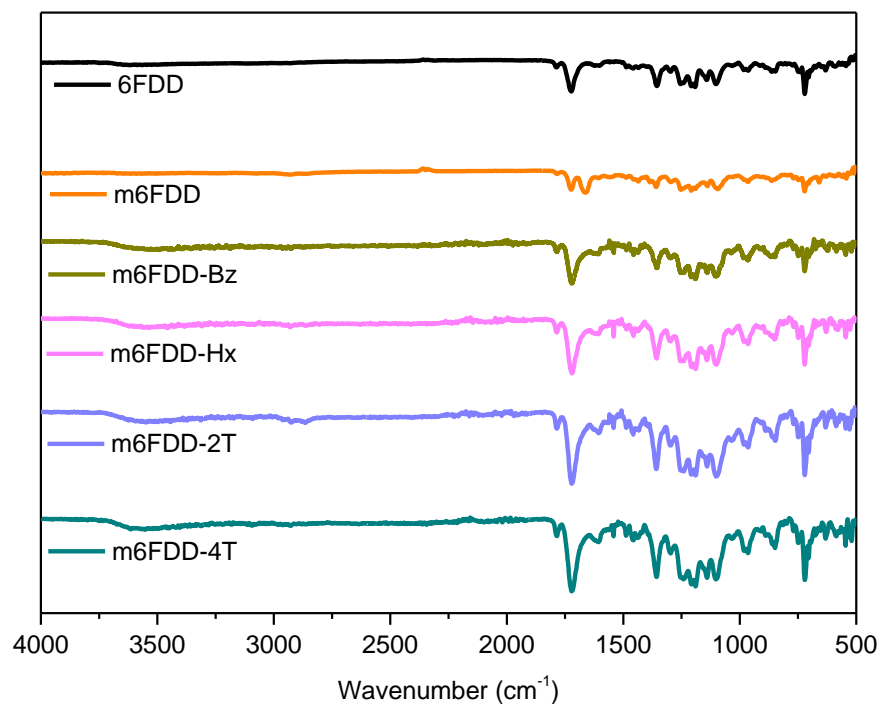


Figure S4. FTIR spectra of obtained from the 6FDD-based membranes (6FDD, black; m6FDD, orange; m6FDD-Bz, olive; m6FDD-Hx, light pink; m6FDD-2T, light blue; m6FDD-4T, turquoise).

Supplementary Photographs

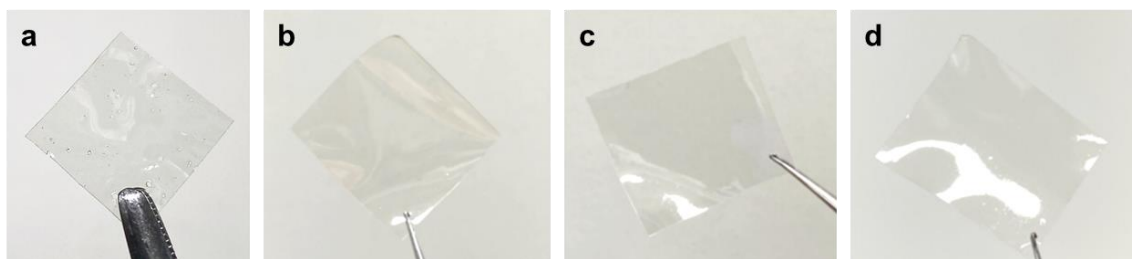


Figure S5. Photographs of the 6FDD-based membranes: (a) m6FDD, (b) m6FDD-Hx, (c) m6FDD-2T, and (d) m6FDD-4T. Each sample size: 3 cm × 3 cm × 70 μm

Tensile Stress–Strain Curves

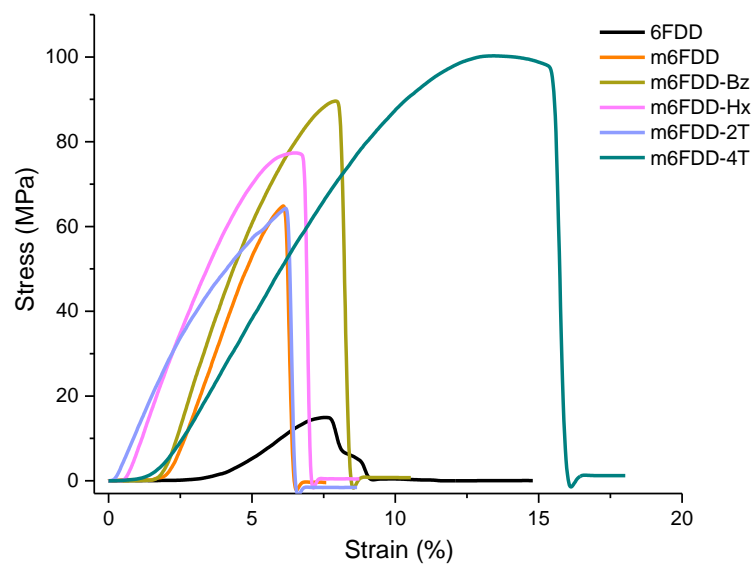


Figure S6. Representative tensile stress–strain curves obtained from the 6FDD-based membranes (6FDD, black; m6FDD, orange; m6FDD-Bz, olive; m6FDD-Hx, light pink; m6FDD-2T, light blue; m6FDD-4T, turquoise).

SEM Images

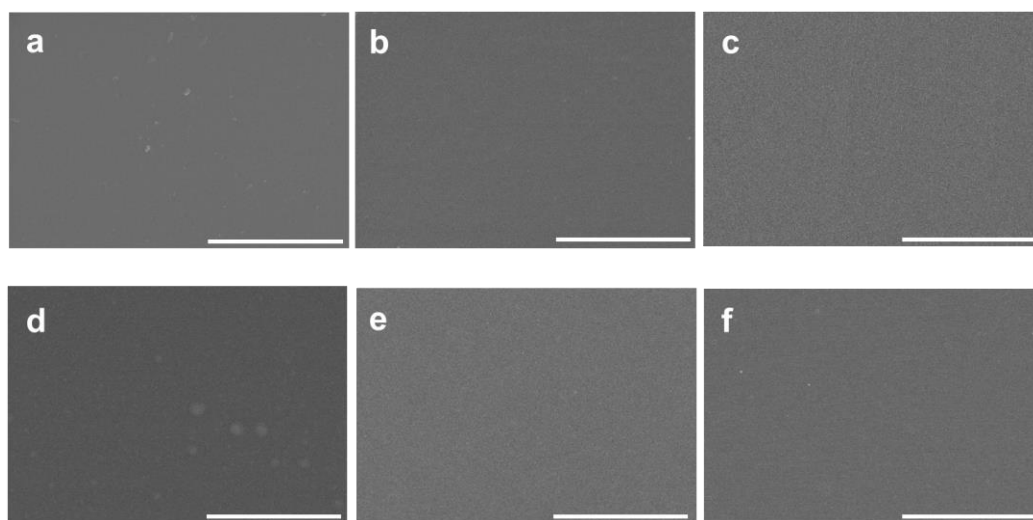


Figure S7. SEM image of 6FDD-based films observed at a magnification of 10000 \times . (top) a: 6FDD; b: m6FDD; c: m6FDD-Bz; (bottom) d: m6FDD-Hx; e: m6FDD-2T; f: m6FDD-4T. A white scale bar indicates 5 μ m.

Contact Angle Measurement

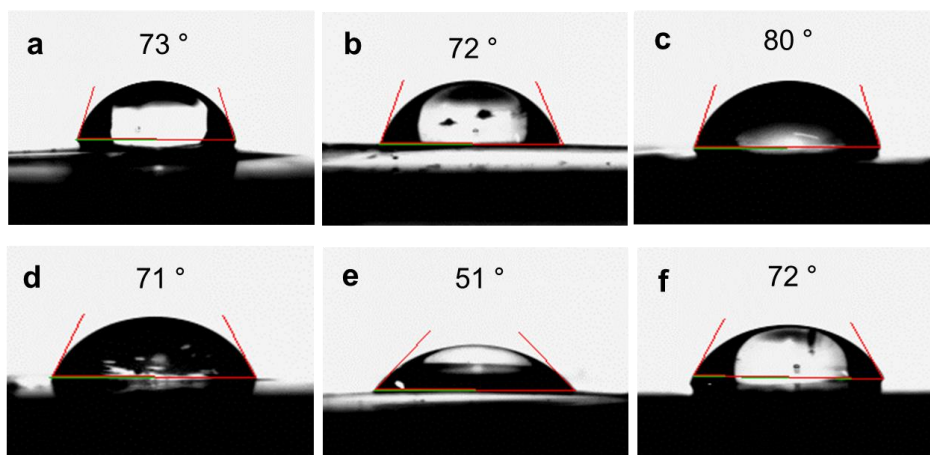


Figure S8. Digital images of each water droplet on the surfaces of the 6FDD-based membranes (a, 6FDD; b, m6FDD; c, m6FDD-Bz; d, m6FDD-Hx; e, m6FDD-2T; f, m6FDD-4T). Average water contact angles are shown on top.

Plasticization Behavior

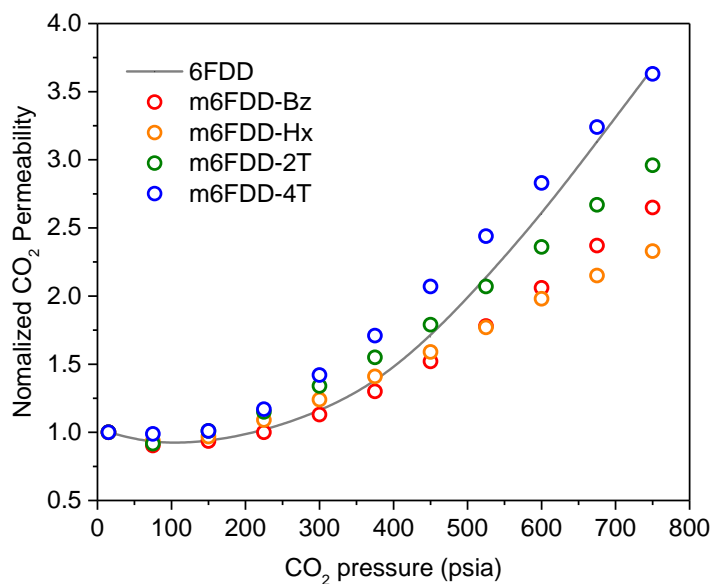


Figure S9. Change in normalized CO₂ permeability of the cross-linked membranes as a function of CO₂ gas feed pressure. The initial CO₂ feed pressure was 15 psi and the second CO₂ feed pressure was 75 psi. After that, the CO₂ feed pressure was gradually increased with 75 psi feed pressure intervals up to 750 psi. The data from the pristine 6FDD are shown for comparison (gray).

Estimation of Fractional Free Volume

Fractional free volume (FFV) of each reinforced membrane was estimated by a ratio of the free volume (V_f) to specific volume ($V = 1/\rho$) as follows:

$$\text{FFV} = V_f/V = (V - 1.3V_w) / V$$

where V and V_w indicate specific molar volume ($\text{cm}^3 \text{ mol}^{-1}$) and van der Waals volume ($\text{cm}^3 \text{ mol}^{-1}$) determined by the Bondi's group contribution method.^{S2}

Gas Permeation Measurement

Pure gas permeation measurement:

Pure gas permeation properties of H_2 , N_2 , CH_4 , and CO_2 gases were measured using a constant-volume, variable-pressure gas permeation system (Maxwell Robotics). The membranes were used to make a coupon using impermeable brass disk with 5-minute epoxy. The specific active area of the membrane was determined using a high-resolution scanner and the Image J software. The coupon was placed in a permeation cell in an oven. The oven temperature was set as 35°C using an air-heating circulator. The permeation system was under dynamic vacuum conditions with the opening of all connected valves without injecting and venting valves. This pretreatment was conducted at least for 6 h to get rid of any residual solvent or chemical species. The leak test was initially performed to calculate the precise gas transport rate by subtracting the leak rate from the measured gas transport rate. The H_2 , N_2 , CH_4 , and CO_2 gases were sequentially injected to make an upstream pressure of 150 psi. In the meantime, the downstream was under a vacuum state. The pure gas permeation properties were measured by opening valves connected to the permeation cell so that the pure gas can transport from upstream to downstream due to the

pressure difference-driven force. The pure gas transport rate in the steady-state is estimated based on at least six times of time lag (θ). The time lag will be explained in the later section.

Gas permeation parameter estimation:

- Pure gas permeability

The pure gas permeability was estimated using the following equation

$$P_i = \frac{Vl}{p_2ART} \left[\left(\frac{dp_i}{dt} \right)_{ss} - \left(\frac{dp_i}{dt} \right)_{leak} \right]$$

where P_i is the pure gas permeability [Barrer ($10^{-10} \cdot \text{cm}^3(\text{STP}) \cdot \text{cm} \cdot \text{cm}^{-2} \cdot \text{s}^{-1} \cdot \text{cmHg}^{-1}$)], V is the downstream volume (cm^3), l is the average thickness of membrane (cm), p_2 is the upstream pressure (cmHg), A is the active area of membrane (cm^2), R is the ideal gas constant, T is the temperature in an oven (K), $(dp_i/dt)_{ss}$ is the increasing rate of downstream pressure in the steady-state (cmHg/s), and $(dp_i/dt)_{leak}$ is the leak rate (cmHg/s).

- Ideal gas selectivity

The ideal gas selectivity ($\alpha_{i/j}$) was calculated as a ratio of the two pure gas permeabilities. In general, the pure gas permeability (P_i) of more permeable gas molecule (i) is divided by the pure gas permeability (P_j) of less permeable gas molecule (j).

- Diffusivity and solubility

The pure gas permeability can be used to interpret the kinetic-(diffusivity) and thermodynamic-(solubility) effects on the gas permeation properties. The pure gas permeability can be divided into two factors (diffusivity and solubility) using the solution-diffusion model as follows.

$$P = \bar{D} \cdot \bar{S}$$

where \bar{D} is the effective diffusivity (cm^2/s) and \bar{S} is the effective solubility ($\text{cm}^3(\text{STP})/\text{cm}^3 \cdot \text{atm}$). In the gas permeation properties, the effective diffusivity correlated to the kinetic parameter, and the effective solubility correlated to the thermodynamic parameter.

The diffusivity can be estimated using the time lag method as follows.

$$D = \frac{l^2}{6\theta}$$

where D is the diffusivity (cm^2/s), l is the average thickness of membrane (cm), θ is the time lag (s)

The solubility can be calculated based on the estimated pure gas permeability and diffusivity using the solution-diffusion model with the simple back-calculation.

The diffusivity-selectivity and solubility-selectivity can be determined as a ratio of two diffusivities and solubilities similar to the calculation method for the ideal gas selectivity.

- Plasticization behavior

The CO_2 plasticization behavior was determined by injecting the CO_2 gas upstream with a gradual feed pressure increase. First, the longest time to reach steady-state for CO_2 gas at 15 psi among all membrane samples was determined. Based on that time, the holding time for CO_2 gas injection at all pressure was determined to guarantee the correct CO_2 transport rate in the steady-state for all membrane samples. After that, the CO_2 gas feed pressure was sequentially increased up to 750 psi with an appropriate pressure interval. The first CO_2 feed pressure was 15 psi and the second CO_2 feed pressure was 75 psi, and then the CO_2 feed pressure increased at 75 psi intervals. The CO_2 permeabilities in the steady-state were

determined at all CO₂ feed pressure. The CO₂ permeabilities were normalized using the first CO₂ permeability at 15 psi to show the relative CO₂ permeabilities for all membrane samples. The relative CO₂ permeabilities exhibit the CO₂ plasticization behavior.

Gas Permeation Properties: Permeability and Selectivity

Table S2. H₂, N₂, CH₄, and CO₂ permeabilities and CO₂/CH₄, CO₂/N₂, H₂/CH₄, H₂/N₂ selectivities at 150 psi and 35 °C of the membrane samples. The unit of permeability is Barrer.

Sample	P(H ₂)	P(N ₂)	P(CH ₄)	P(CO ₂)	P(CO ₂)/P(CH ₄)	P(CO ₂)/P(N ₂)	P(H ₂)/P(CH ₄)	P(H ₂)/P(N ₂)
6FDD	116	3.32	2.09	78.2	37.4	23.5	34.8	55.4
m6FDD	237	9.46	6.11	199	32.7	21.1	38.8	25.0
m6FDD-Bz	107	2.52	1.48	67.0	45.3	26.6	42.3	72.1
m6FDD-Hx	70	1.53	0.95	37.7	39.9	24.6	45.7	74.2
m6FDD-2T	53	1.39	0.97	33.3	34.5	24.0	38.3	54.9
m6FDD-4T	30	0.48	0.29	13.0	45.2	27.0	61.5	103.0

Gas Permeation Properties: Diffusivity and Diffusivity-Selectivity

Table S3. N₂, CH₄, and CO₂ diffusivities and CO₂/CH₄, CO₂/N₂, diffusivity-selectivities at 150 psi and 35 °C of the membrane samples. The unit of diffusivity is 10⁻⁷ cm²/s.

Sample	D(N ₂)	D(CH ₄)	D(CO ₂)	D(CO ₂)/D(CH ₄)	D(CO ₂)/D(N ₂)
6FDD	0.388	0.0916	0.702	7.66	1.81
m6FDD	0.99	0.23	2.05	8.91	2.07
m6FDD-Bz	0.295	0.0606	0.534	8.81	1.81
m6FDD-Hx	0.256	0.0506	0.393	7.77	1.54
m6FDD-2T	0.199	0.0468	0.359	7.67	1.80
m6FDD-4T	0.118	0.0226	0.177	7.83	1.50

Gas Permeation Properties: Solubility and Solubility-Selectivity

Table S4. N₂, CH₄, and CO₂ solubilities and CO₂/CH₄, CO₂/N₂, solubility-selectivities at 150 psi and 35 °C of the membrane samples. The unit of solubility is cm³(STP)/cm³·atm

Sample	S(N ₂)	S(CH ₄)	S(CO ₂)	S(CO ₂) /S(CH ₄)	S(CO ₂) /S(N ₂)
6FDD	0.651	1.73	8.46	4.89	13.0
m6FDD	0.73	2.03	7.38	3.64	10.1
m6FDD-Bz	0.648	1.85	9.53	5.15	14.7
m6FDD-Hx	0.455	1.42	7.30	5.14	16.0
m6FDD-2T	0.530	1.57	7.05	4.49	13.3
m6FDD-4T	0.310	0.972	5.59	5.75	18.0

References

- S1. Shindo, R.; Amanuma, S.; Kojima, K.; Sato, S.; Kanehashi, S.; Nagai, K. Characterization and Gas Permeation Properties of UV-Cured Fluorine-Containing Telechelic Polyimide Membranes with a Crosslinker. *Polym. Eng. Sci.*, **2014**, *54*, 1089–1099.
- S2. Zhang, C.; Li, P.; Cao, B. Decarboxylation crosslinking of polyimides with high CO₂/CH₄ separation performance and plasticization resistance. *J. Memb. Sci.*, **2017**, *528*, 206–216.
- S3. Zhang, C.; Cao, B.; Li, P. Thermal oxidative crosslinking of phenolphthalein-based cardo polyimides with enhanced gas permeability and selectivity. *J. Memb. Sci.*, **2018**, *546*, 90–99.
- S4. Park, J. S.; Gleason, K. L.; Gaines, K. E.; Mecham, S. J.; McGrath, J. E.; Freeman, B. D. Effect of UV crosslinking on transport properties of CO₂ and N₂ through poly(imide-siloxane) segmented copolymer. *Energy Procedia*, **2014**, *63*, 210–216.
- S5. Wang, H.; Zhang, K.; Li, J. P. H.; Huang, J.; Yuan, B.; Zhang, C.; Yu, Y.; Yang, Y.; Lee, Y.; Li, T. Engineering plasticization resistant gas separation membranes using metal-organic nanocapsules. *Chem. Sci.*, **2020**, *11*, 4687–4694.
- S6. Wind, J. D.; Staudt-Bickel, C.; Paul, D. R.; Koros, W. J. The Effects of Crosslinking Chemistry on CO₂ Plasticization of Polyimide Gas Separation Membranes. *Ind. Eng. Chem. Res.*, **2002**, *41*, 6139–6148.
- S7. Iwasa, R.; Suizu, T.; Yamaji, H.; Yoshioka, T.; Nagai, K. Gas separation in polyimide membranes with molecular sieve-like chemical/physical dual crosslink elements onto the top of surface. *J. Memb. Sci.*, **2018**, *550*, 80–90.

- S8. Ma, C.; Koros, W. J. High-performance ester-crosslinked hollow fiber membranes for natural gas separations. *J. Memb. Sci.*, **2013**, *428*, 251–259.
- S9. Gnanasekaran, D.; Walter, P. A.; Parveen, A. A.; Reddy, B. S. R. Polyhedral oligomeric silsesquioxane-based fluoroimide-containing poly(urethane-imide) hybrid membranes: Synthesis, characterization and gas-transport properties. *Sep. Purif. Technol.*, **2013**, *111*, 108–118.
- S10. Li, S.; McGinness, H.; Wang, T.; Guo, R. Crosslinked Matrimid®-like polyimide membranes with unimodal network structure for enhanced stability and gas separation performance. *Polymer*, **2021**, *237*, 124323.
- S11. Wu, C.-Y.; Hu, C.-C.; Lin, L.-K.; Lai, J.-Y.; Liu, Y.-L. Liberation of small molecules in polyimide membrane formation: An effect on gas separation properties. *J. Memb. Sci.*, **2016**, *499*, 20–27.
- S12. Yu, S.; Li, S.; Wang, H.; Zhu, C.; Hou, J.; Cui, S.; Shen, X.; Liu, Y. Crosslinked microporous polyarylate membranes with high Kr/Xe separation performance and high stability under irradiation. *J. Memb. Sci.*, **2020**, *611*, 118280.
- S13. Kwisnek, L.; Heinz, S.; Wiggins, J. S.; Nazarenko, S. Multifunctional thiols as additives in UV-cured PEG-diacrylate membranes for CO₂ separation. *J. Memb. Sci.*, **2011**, *369*, 429–436.
- S14. Kline, G. K.; Weidman, J. R.; Zhang, Q.; Guo, R. Studies of the synergistic effects of crosslink density and crosslink inhomogeneity on crosslinked PEO membranes for CO₂-selective separations. *J. Memb. Sci.*, **2017**, *544*, 25–34.
- S15. Chen, Y.; Qin, J.; Tong, T.; Zhou, H.; Cao, X.; Jin, W. Study on the effect of cross linking temperature on microporous polyamide membrane structure and its nitrogen/cyclohexane separation performance. *Sep. Purif. Technol.*, **2020**, *252*, 117401.
- S16. Harrigan, D. J.; III, J. A. L.; Reid, H. W.; Rivers, J. B.; O'Brien, J. T.; Sharber, S. A.; Sundell, B. J. Tunable sour gas separations: Simultaneous H₂S and CO₂ removal from natural gas via crosslinked telechelic poly(ethylene glycol) membranes. *J. Memb. Sci.*, **2020**, *602*, 117947.